



Transition Strategy Optimization of Inconel625-HSLA Steel Functionally Graded Material Fabricated by Wire Arc Additive Manufacturing

Jiarong Zhang¹ · Chengning Li^{1,2} · Lingzhi Ba¹ · Xinjie Di^{1,2}

Received: 26 March 2022 / Accepted: 18 May 2022 / Published online: 17 June 2022
© The Author(s) under exclusive licence to The Korean Institute of Metals and Materials 2022

Abstract

Functionally graded material (FGM), showing special regular structural and performance changes along specific direction, is appropriate to be fabricated by wire arc additive manufacturing (WAAM). And Inconel625-high strength low alloy (HSLA) steel FGM has potential for replacing the dissimilar joints to avoid the drastic variation in the multi-material interface. However, due to the continuity of compositional change, the Inconel625-HSLA steel FGM fabricated by WAAM with iso-variable transition strategy (ITS) would contain the graded regions with weak performance or detrimental precipitates. Whereas these unfavourable graded regions can be addressed through transition strategy optimization. In this research, an optimized transition strategy (OTS) was applied to modify the Inconel625-HSLA steel FGM fabricated by WAAM. Weak-performance graded regions of the FGM fabricated by ITS were eliminated by OTS. Microstructures, precipitation behavior and mechanical properties in room-temperature and 700 °C of the FGMs manufactured in two transition strategies were compared. The effect of Laves phases in mechanical properties of the FGM was clarified. After using OTS, the average room-temperature tensile strength of the FGM was improved from 449 to 509 MPa, and average tensile strength in 700 °C was improved from 403 to 464 MPa.

Keywords Functionally graded material · Additive manufacturing · Transition strategy · Laves phase · Mechanical properties

1 Introduction

Inconel625 alloy exhibits outstanding performances of corrosion resistance, fatigue, wear and thermal properties [1–3], and HSLA (high-strength low alloy) steel shows prominent mechanical performances [4, 5]. The dissimilar welding joints of these two materials have been widely used in service environments with harsh requirement such as petrochemical factories and heat exchange tube junction in nuclear engineering plant where a combination of strength and corrosion resistance is required [6, 7]. Nevertheless, the joints performances are usually deteriorated by the

drastic variation in multi-material interface caused by large discrepancies of linear expansion coefficients and melting points [8–10]. Whereas functionally graded material (FGM), a material series with structures and properties smoothly transiting along specific direction, is perfectly suitable for jointing different alloys and is potential to substitute the dissimilar welding joints of nickel alloy and HSLA steel [11].

Traditional manufacturing process of FGM can be classified into gas-based procedures (such as chemical vaporization), liquid phase process (such as directional solidification and laser deposition) and solid phase technologies (such as thermal pressing) [12, 13]. In comparison with these manufacturing procedures, additive manufacturing (AM), with its particularities of layer-by-layer productive process, shows huge advantages as a manufacturing process to fabricate FGM in chemical composition controlling, shaping regulation, production efficiency and economy. Varun et al. [14] manufactured Ni–Fe and Co–Fe based magnetic graded material by laser-powder additive manufacturing, achieving the controlling of remanent magnetization gradient change

✉ Xinjie Di
dixinjie@tju.edu.cn

¹ School of Materials Science and Engineering, Tianjin University, Tianjin 300350, China

² Tianjin Key Laboratory of Advanced Joining Technology, Tianjin 300350, China

along building direction. The aforementioned AM-FGM manufacturing technologies were mainly laser-powder-based AM process, which is capable of controlling materials content accurately and fabricating complicated-structure products. However, due to low deposition rate (less than 1.0 kg/h), long productive time and high material cost, it is impractical to manufacture large-size workpieces by these methods. Nevertheless, wire arc additive manufacturing (WAAM), contributing to its advantage of high-efficiency (with deposition rate over 3.0 kg/h), lower fabrication cost (lower price of wires than of powder), lower oxide contamination (smaller surface areas of wires than of powder) [15–18] and high deposition energy, conforms with the requirements of fabricating components with large size and full-density in nuclear and marine engineering, and shows the technical superiority of manufacturing Inconel625-HSLA steel FGM. As for Ni-based alloy and steel single ingredient materials, several studies have been reported. Seow et al. [19] fabricated Inconel718 by WAAM and studied the effect of heat treatments on the components. Wang et al. [20] used WAAM to manufacture Inconel625, summarizing the microstructure and precipitation in different position. Li et al. [21] fabricated low-carbon steel by WAAM, achieving the regulation of heat process during the fabrication. Wu et al. [22] compared the effect of welding current and arc strategy on the stainless-steel components fabricated by WAAM. Nevertheless, rare researches of fabricating Ni-based and steel FGM by WAAM have been reported albeit the significant advantages.

Contraposing FGM, composition changes along the building direction, leading to the microstructure and properties discrepancy. Therefore, composition variation has a significant effect on FGM performance. Bobbio et al. [23, 24] investigated Invar 36/Ti-6Al-4 V FGM in which Ti-6Al-4 V was linearly graded to Invar 36 in 3% increments. Nevertheless, Ni-Ti and Fe-Ti intermetallic both generated and induced the strength decreasing. Meng et al. [25] fabricated Inconel625-Ti6Al4V FGM by 10% Ti6Al4V increments. However, many cracks occurred in the graded region between 80% Inconel625 and 70% Inconel625. Shen et al. [26] fabricated Fe-Fe₃Ni FGM by WAAM with a 5% of Ni increments. But there was a drastic mechanical properties changes between the adjacent graded layers. By eliminating weak performance graded regions, transition strategy optimization is available for alleviating the adverse effects caused by composition variation of FGMs. Pulugurtha [27] compared Inconel625-Ti6Al4V FGMs fabricated in different transition strategies and illustrated that the gradient path in which Ti6Al4V transitions to 50% Inconel625 in 10% steps followed by a direct jump to 100% Inconel625 would avoid the brittle TiNi precipitation. Chen et al. [28] fabricated AlN-Mo FGMs with transition strategies of grading 100%AlN to 100%Mo at 5%, 10% and 20% intervals and

declared that the AlN-Mo FGM fabricated in strategy with 5% intervals shows the best bending strength.

Although transition strategy optimization shows evident advantages in microstructure design and properties increase-ment of FGM, the researches of this topic are very rare. Especially for nickel alloy and steel FGM, notwithstanding the fabrication of graded component [29, 30], few study of transition strategy optimization has been reported. According to our previous research on fabricating Inconel625-HSLA steel FGM by WAAM [31], precipitation of Laves phases and graded regions with weak mechanical properties would be mightily detrimental to the material performances. Therefore, in order to improve the comprehensive properties of Inconel625-HSLA steel FGM, an optimized transition strategy was applied in WAAM process to eliminate the poor performances graded regions.

2 Materials and Methods

The WAAM system was shown in Fig. 1a. The substrates and wires were cleaned before the fabrication. Argon gas (99.99%) with a flow of 20L/min was used as the oxidation prevention gas. 1.2 mm diameter Inconel625 and HSLA steel wires were utilized in WAAM as the filler metals. Q345 steel plate of 250 mm × 200 mm × 20 mm (length × width × thickness) was used as the substrate. The average chemical compositions of the wires were tested by X-ray fluorescence spectrometer (XRF-1800) and showed in Table 1. The wire with higher feeding speed was kept in the upper location. The voltage was kept in 13–14 V. The welding current was 140A when the feeding speed of Inconel625 wire was higher and that was 130A when the feeding speed of HSLA steel wire was higher. As showing Fig. 1b, the building direction was perpendicular to the substrate and the scanning direction was parallel to the substrate. The scanning speed was 1.5 mm/s, and the total feeding speed of two wires was 1.5 m/min. The tensile strength was tested along the building direction and the specimen dimension of which was illustrated in Fig. 1b.

Figure 2 shows the schematic of the test samples. The sample in Fig. 2a was fabricated by WAAM with iso-variable transition strategy (ITS), in which the content of HSLA steel was increased by 10% per layer. And based on our previous studies on Inconel625-HSLA steel FGM manufactured by WAAM [31], the graded region with 70% Inconel625-30% HSLA steel included plentiful Laves phases which is detrimental to FGM, and the graded region with 30% Inconel625-70% HSLA steel showed the weakest tensile strength. Therefore, in this study, these poor performance grade regions were eliminated. Furthermore, considering the element diffusion which would mix the composition from adjacent layers, the graded regions with

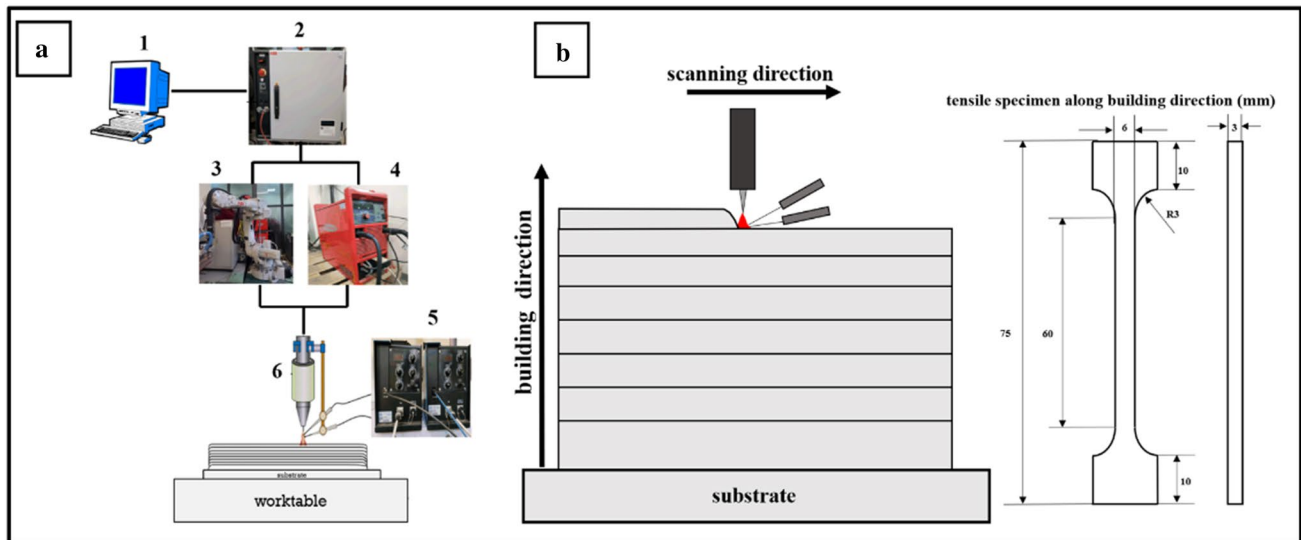


Fig. 1 **a** WAAM with EMS system: computer control system (1), controlling box (2), ABB 6-axis robot (3), Fronius TIG-5000 (4), wires feeding system (5), welding gun (6), **b** Schematic of WAAM process and tensile specimens

Table 1 Chemical composition of Inconel625 and HSLA steel deposited metal (wt%)

Element	C	Si	Mn	Fe	Cr	Mo	Ti	Nb	Ni
Inconel625	0.037	0.056	0.027	0.25	22.25	8.97	0.17	3.73	Bal
HSLA steel	0.054	0.41	1.37	Bal	0.033	0.24	0.013	-	0.48

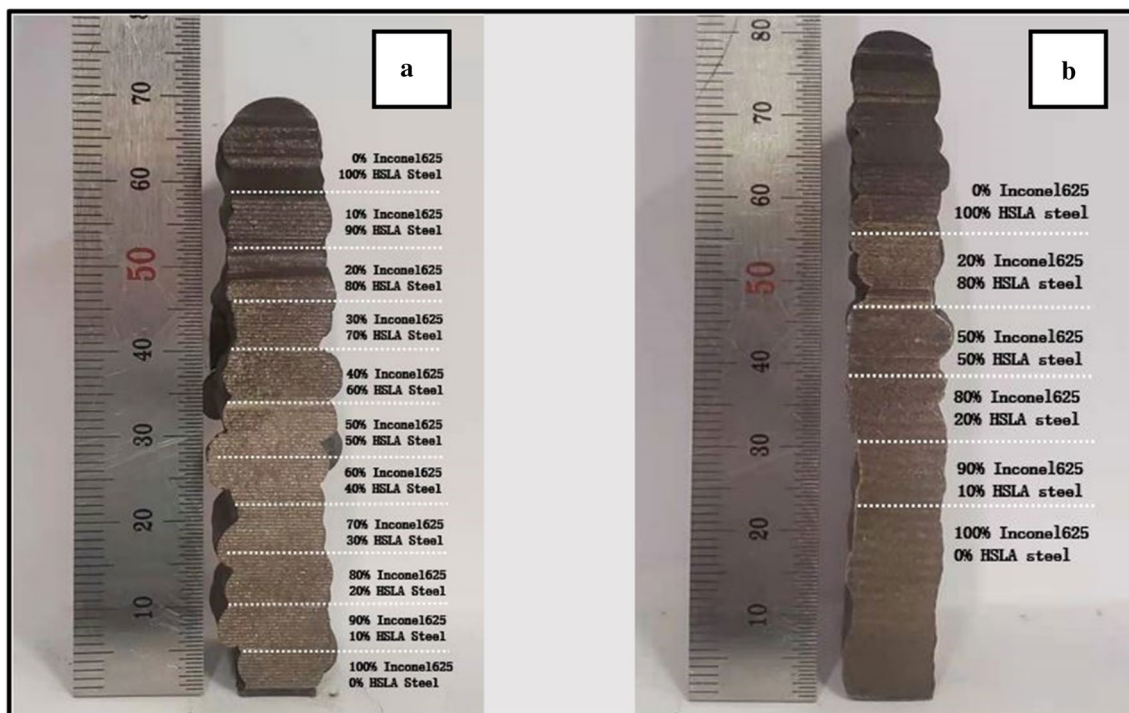


Fig. 2 **a** sample ITS fabricated by WAAM with iso-variable transition strategy, **b** sample OTS fabricated by WAAM with optimized transition strategy

40% Inconel625-60% HSLA steel and 60% Inconel625-40% HSLA steel were also eliminated. The FGM sample fabricated in this optimized transition strategy (OTS) was shown in Fig. 2b. The sample in Fig. 2a and Fig. 2b would be denoted respectively as sample ITS and sample OTS in following.

Aqua regia solution (30 ml HCL, 10 ml HNO₃) and ethyl alcohol solution (10 ml HNO₃, 50 ml ethyl alcohol) were used respectively to etch the specimens of the graded regions with Inconel625 wire feeding speed ≥ 0.45 m/min and that of < 0.45 m/min. All the specimens were subsequently cleaned ultrasonically. Optical microscope (OM), scanning electron microscope (SEM), energy dispersive spectroscopy (EDS) and transmission electron microscope (TEM) were used to observe the microstructures. Tensile strength in room temperature and 700°C were tested to compare the mechanical properties of the two samples. The tensile strength was tested by MTS Model E45, and the DIC system was PELICAN 1650 CASE.

3 Results and Discussions

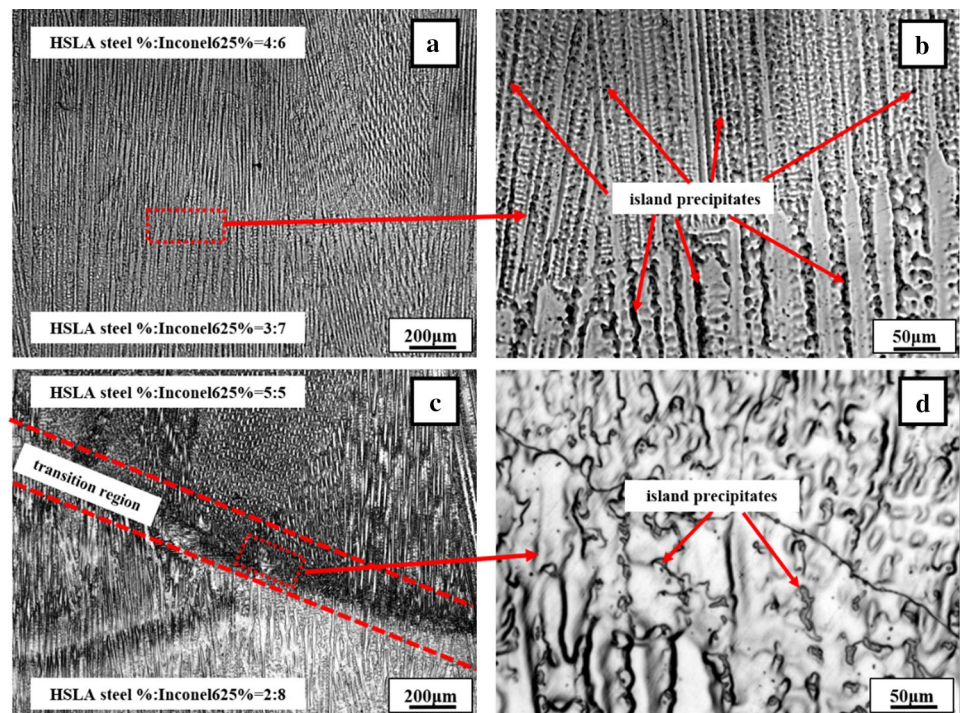
3.1 Microstructure

The comparison of microstructures of sample ITS and sample OTS was shown in Fig. 3. As shown in Fig. 3a, c, the microstructure of the FGMs were columnar dendrites as result of the directional heat dissipation opposite to the

building direction and the partially remelting of previously layer during WAAM [32]. As for sample ITS, substantial island precipitates generated in the graded regions with 30% HSLA steel-70% Inconel625 and 40% HSLA steel-60% Inconel625 (Fig. 3b). While in sample OTS these two graded regions were removed by the optimized transition strategy, replaced by a transition region between the graded region with 20% HSLA steel-80% Inconel625 and that with 50% HSLA steel-50% Inconel625. Comparing the two graded region layers in sample ITS and the transition region, sporadically distributing island precipitates notwithstanding (Fig. 3d), of sample OTS, the island precipitates generation area of the FGM has been greatly narrowed by the optimized strategy.

The SEM images for the island precipitates in the sample ITS were shown in Fig. 4a, and the element mapping illustrates that the island precipitates were rich in Mo and Nb. As shown Fig. 4b, EDS result of the position marked with the red cross in Fig. 4a illustrated that the atom percentage of Ni, Fe and Cr was 53.29 and that was 34.84 for Nb and Mo, indicating that the island precipitates was closed to AB₂ type Nb and Mo rich phase. Figure 4c, d showed the bright field TEM micrograph and the selected area electron diffraction (SAED) pattern of the island precipitates separately. The island precipitates with a size of about 600 nm showed a hexagonal close-packed crystal system. The combining analysis of the EDS and TEM confirmed that the island precipitates in the FGMs were (Ni, Fe, Cr)₂(Mo, Nb) type Laves phases that were caused by the segregation of

Fig. 3 Microstructures of the FGMs: **a** graded regions with 30% HSLA steel-70% Inconel625 and 40% HSLA steel-60% Inconel625 of sample ITS, **b** island precipitates generated in the both graded regions, **c** the transition region between the graded region of 20% HSLA steel-80% Inconel625 and 50% HSLA steel-50% Inconel625 in sample OTS, **d** island precipitates in the transition region of sample OTS



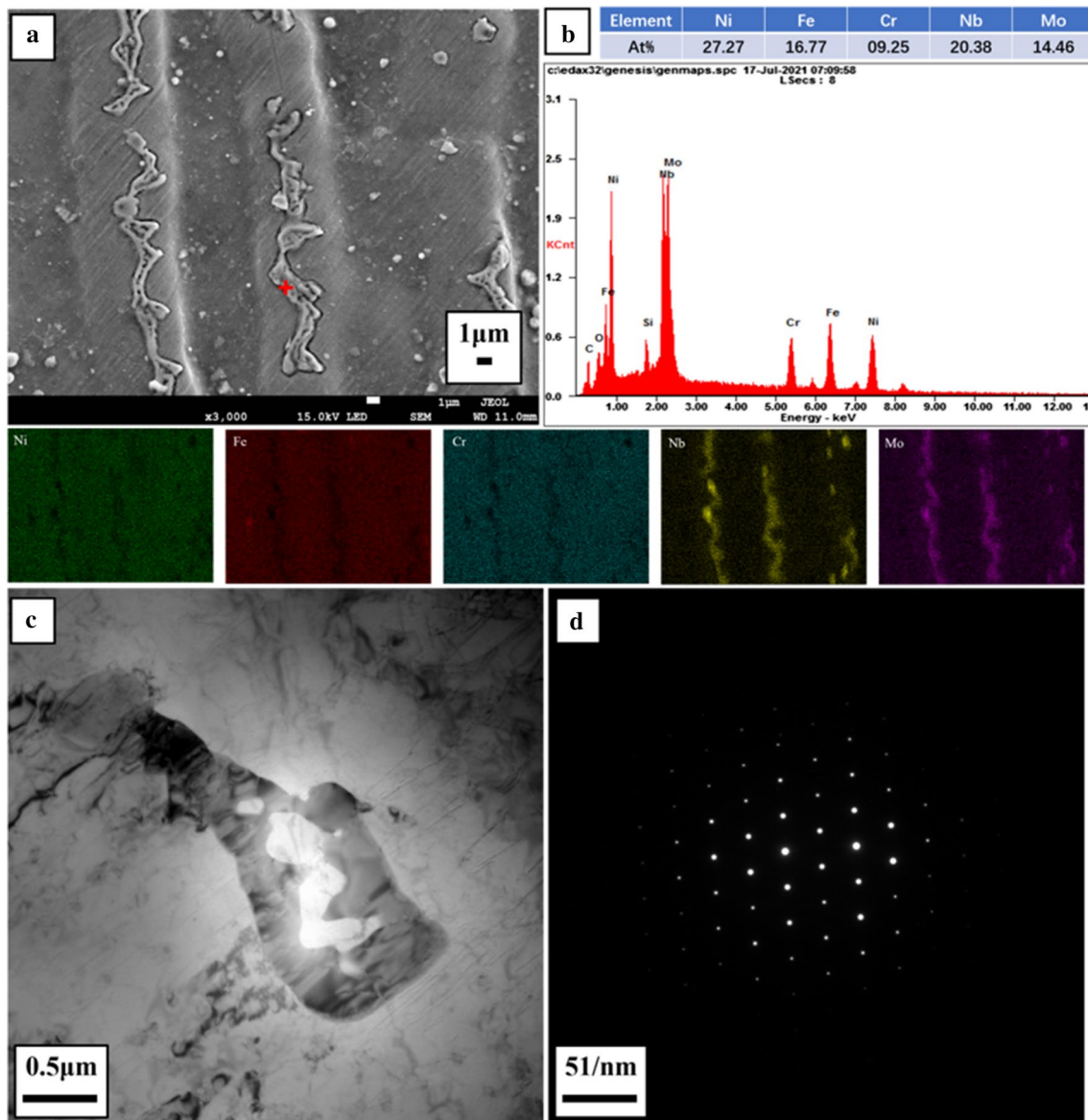


Fig. 4 **a** SEM and element mapping for the island precipitates, **b** EDS result of the position marked with the red cross in **a**, **c** Bright field TEM micrograph of the island precipitates, **d** The selected area electron diffraction (SAED) pattern from [1_21_3]

solution elements during the solidification and harmful to the performance of the FGM.

Compared to the graded regions of 60% HSLA steel-40% Inconel625 and 70% HSLA steel-30% Inconel625 in sample ITS, as shown in Fig. 5a, b, the transition area of graded regions with 50% HSLA steel-50% Inconel625 and 80% HSLA steel-20% Inconel625 in sample OTS (Fig. 5c) obtained lots of granular precipitates. As shown in Fig. 5d, EDS result of the position marked with the red cross in Fig. 5c indicated that the precipitates were rich of Nb and C. The TEM micrograph in Fig. 5e, f illustrated that the precipitates in the sample OTS were face-centered cubic structure. Therefore, combing with SEM and TEM, the precipitates

in the sample OTS could be MC-type Nb-rich carbides. As shown in Fig. 4e, a large number of dislocations gathered around the precipitate, which proved its ability to hinder dislocation migration.

3.2 Mechanical Properties

The tensile strength along building direction of the FGMs were shown in Fig. 6a. The tensile strength, yield strength and elongation of sample ITS and OTS were listed in Table 2. The average tensile strength of sample ITS and OTS were separately 449 MPa and 509 MPa, and the average yield strength of sample ITS and OTS were 270 MPa and

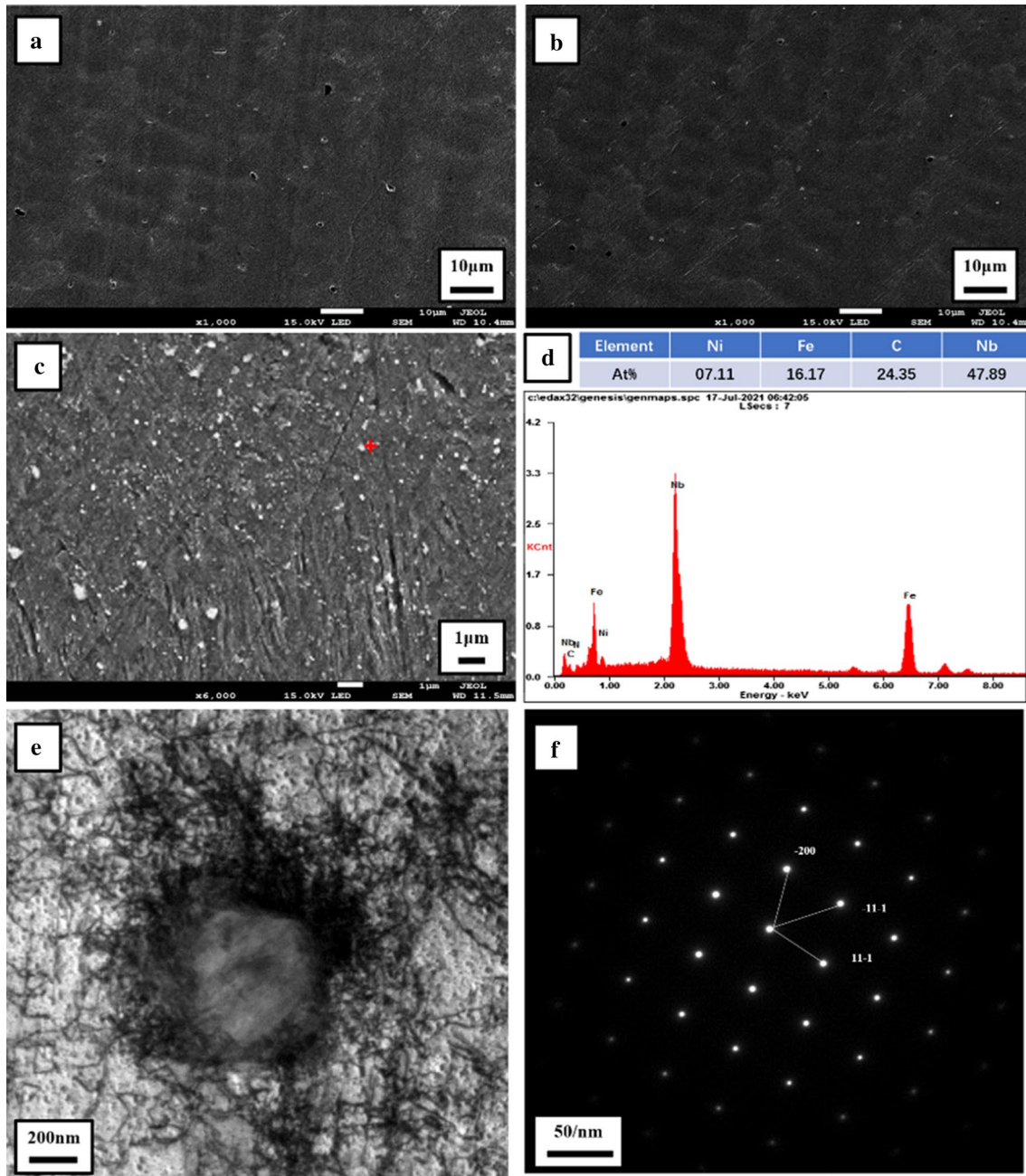


Fig. 5 **a** SEM for the precipitates in graded region of 60% HSLA steel and 40% Inconel 625 in sample ITS, **b** SEM for the precipitates in graded region of 70% HSLA steel and 30% Inconel 625 in sample ITS, **c** SEM for the precipitates in the transition region between the graded region of 20% HSLA steel-80% Inconel and 50% HSLA steel-

50% Inconel in sample OTS, **d** EDS result of the position marked with the red cross in **c**, **e** Bright field TEM micrograph of the Nb-rich precipitates, **f** The selected area electron diffraction (SAED) pattern from [011]

340 MPa separately. As shown in Fig. 6b, during stretching process, the stress concentration position of sample ITS was the graded region of 70% HSLA steel-30% Inconel 625 which was also the fracture position, demonstrating the graded region of 70% HSLA steel-30% Inconel 625 as the weakest graded layer. While after applying optimized transition strategy, showing in Fig. 6c, the stress concentration and

fracture position during stretching process transferred to the graded region with 50% HSLA steel and 50% Inconel 625.

The improvement of tensile strength of the FGMs could be attributed to the elimination of the weak strength graded regions by optimized transition strategy. During WAAM process, the content of solid solution strengthening elements in the FGM from Inconel625 alloy would decrease as HSLA

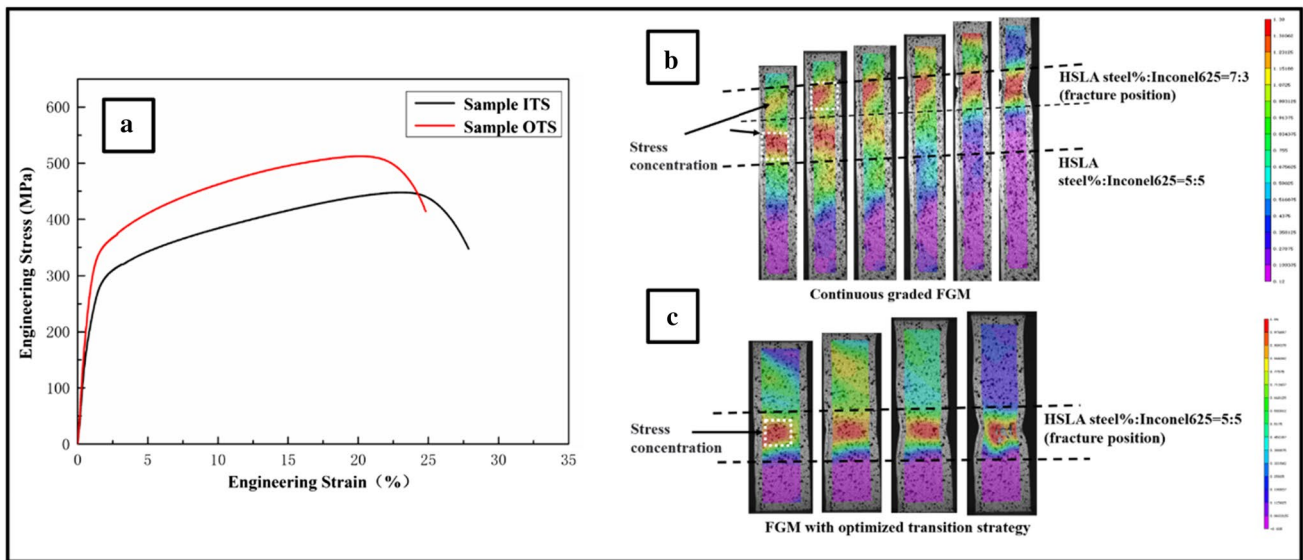


Fig. 6 Mechanical properties of the FGMs: **a** engineering stress–strain curve, **b** DIC test of sample ITS, **c** DIC test of sample OTS

Table 2 Room-temperature mechanical properties of sample ITS and sample OTS

Properties	Tensile strength (MPa)	Yield strength (MPa)	Elongation (%)
Sample ITS	448 ⁺¹³ ₋₁₀	270 ⁺⁸ ₋₁₁	31.5 ⁺¹ ₋₁
Sample OTS	512 ⁺⁹ ₋₁₆	340 ⁺¹² ₋₁₁	28.0 ^{+1.5} ₋₁

steel replaced Inconel625 alloy. Therefore, the graded region with 70% HSLA steel-30% Inconel625 expressed a weak tensile strength. While in sample OTS the transition region of 80% HSLA steel-20% Inconel625 and 50% HSLA steel-50% Inconel625, substantial Nb-rich carbides precipitated and hindered dislocation migration, improving the tensile strength.

Contraposing wire arc additive manufacturing, as shown in Fig. 7a, the columnar dendrite growing direction was reverse to the heat dissipation direction which was from the welding pool to the substrate and therefore the top of welding pool would be the latest solidification area during manufacturing [33–35]. While the balanced distribution coefficient *K* of Nb is less than 1, which indicates that the solubility of Nb in solid phase is less than that in liquid phase, leading Nb to concentrate from solid to liquid phase during the solidification [36, 37]. Thus, Nb would be inclined to concentrate on the top of the welding pool during solidification. As a result, when fabricating the graded region with 80% HSLA steel-20% Inconel625, the Nb gathered in top area would combine with the C in HSLA steel to form Nb-rich precipitates (shown in Fig. 5). Ulteriorly, as the XRD result illustrated in Fig. 7b, the mainly composition

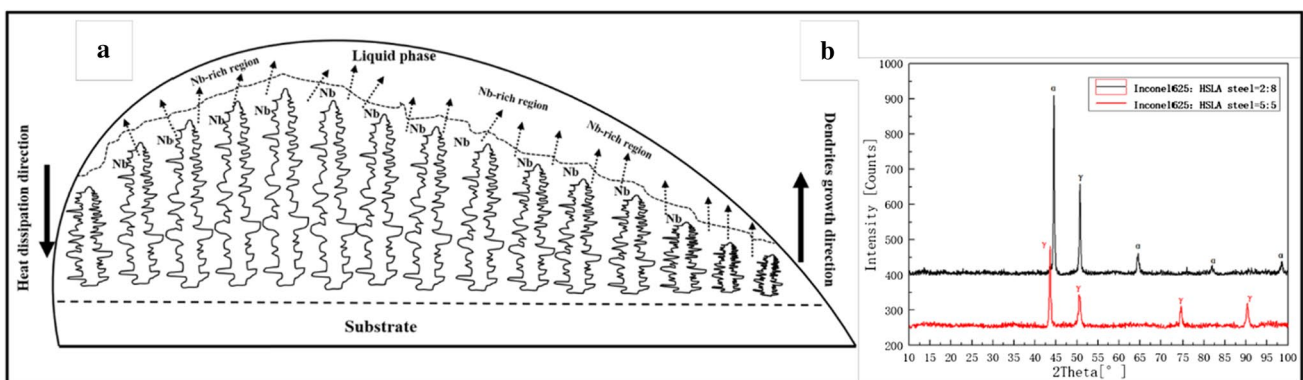


Fig. 7 **a** Schematic diagram of Nb precipitating, **b** XRD result of graded region of 20% Inconel625-80% HSLA steel and 50% Inconel625-50% HSLA steel

of the graded region with 50% HSLA steel-50% Inconel 625 and that with the mainly composition of the graded region of 80% HSLA steel-20% Inconel 625 were respectively γ phase and α phase. The solid solubility of NbC in γ phase and α phase satisfy the formula 1 and formula 2 respectively [38, 39]:

$$\text{Log}\{[\text{Nb}] \cdot [\text{C}]^{0.87}\}_{\gamma} = 3.40 - 7200/T \quad (1)$$

$$\text{Log}\{[\text{Nb}] \cdot [\text{C}]^{0.87}\}_{\alpha} = 5.43 - \frac{10960}{T} \quad (2)$$

The solution rate of Nb-rich carbides in α is less than that of γ when the temperature decreased to 1011 °C. Hence, the solution rate of Nb-rich carbides in the transition region of 20% HSLA steel graded region and 80% HSLA steel graded region would be less than that in 50% HSLA steel graded region and thus induced the generation NbC. To sum up, after using optimized transition strategy, the weak tensile strength graded region of the FGM was removed, and because of the segregation of Nb in solidification and the discrepancy of NbC in the different graded layers, the transition of graded region with 50% HSLA steel-50% Inconel 625 and that with 80% HSLA steel-20% Inconel 625 generated a mass of NbC which would hinder the dislocation migration and thus lead to the improvement of tensile strength of the transition area.

The tensile tests along building direction at 700 °C of sample ITS and sample OTS were illustrated in Fig. 8. The fracture location of sample ITS was graded region of 30%

HSLA steel-70% Inconel625, whereas that of sample OTS was 50% HSLA steel-50% Inconel625 which is corresponding to the fracture position in room temperature. The relative mechanical properties were listed in Table 3. After using optimized transition strategy, the average tensile strength at 700 °C increased from 403 MPa (sample ITS) to 464 MPa (sample OTS), and the average yield strength increased from 195 MPa (sample ITS) to 289 MPa (sample OTS). As shown in Fig. 8b, c, the fracture features of the FGMs were dimples. Unlike sample OTS (Fig. 8c), there were substantial precipitates in the dimples of sample ITS (Fig. 8b), indicating that these precipitates could be responsible for the fracture. As shown in Fig. 8e, the EDS result of the position marked with the red cross in Fig. 8d proved that the precipitates generated around the cracks were Laves, denoting Laves phases the initial position of cracks.

Laves phases in the sample ITS could be accounted for the difference of fracture positions in room-temperature and high-temperature tensile test. Because of consumption of solution elements such as Ni, Mo and Nb, solid solution elements barren areas with lower strength would appear

Table 3 Room-temperature \pm mechanical properties of sample ITS and sample OTS

Properties	Tensile strength (MPa)	Yield strength (MPa)	Elongation (%)
Sample ITS	401 ⁺¹³ ₋₈	196 ⁺¹⁰ ₋₁₂	36.0 ^{+1.5} _{-1.5}
Sample OTS	463 ⁺¹⁴ ₋₁₁	288 ⁺¹⁰ ₋₇	29.5 ⁺¹ ₋₁

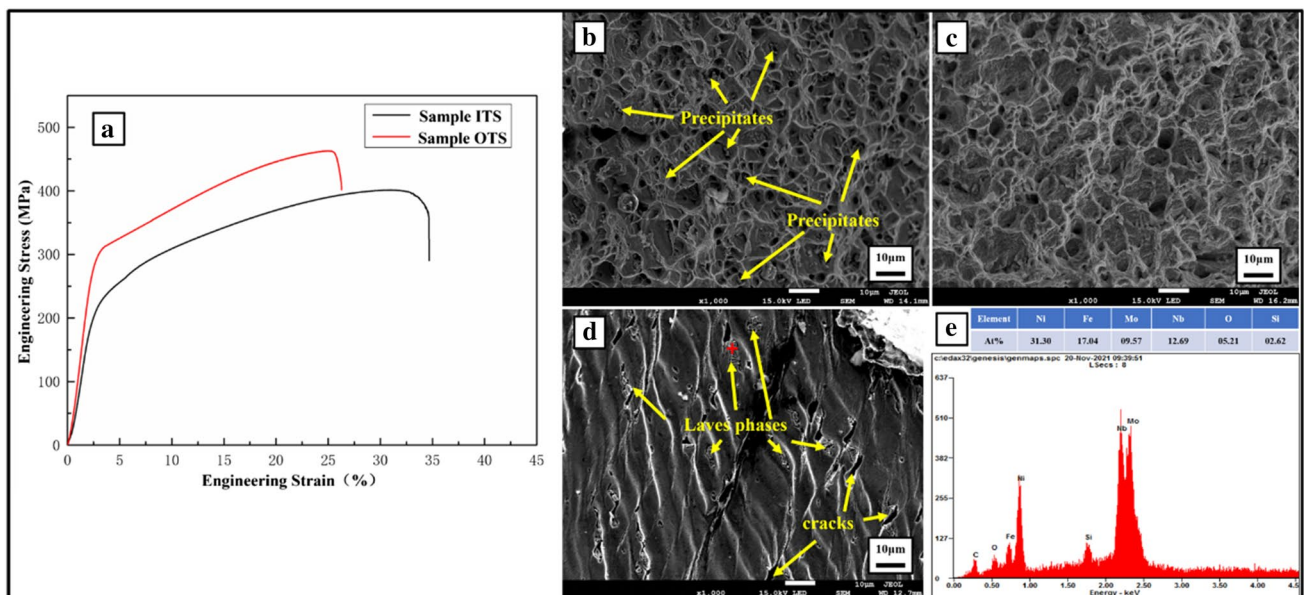
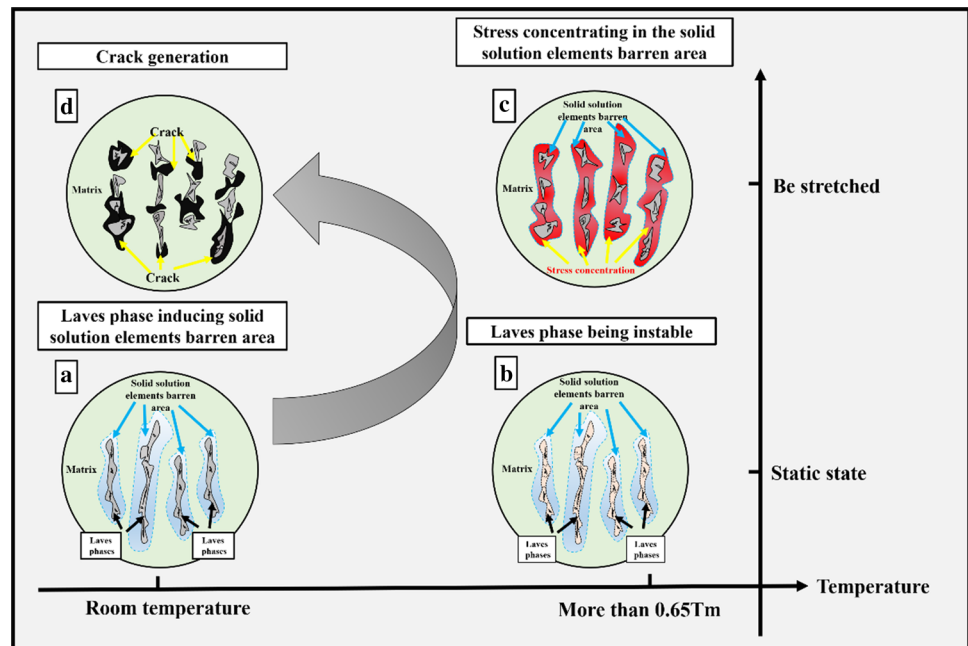


Fig. 8 High-temperature mechanical properties of the FGMs: **a** high-temperature engineering stress–strain curve, **b** fracture surface of sample ITS, **c** fracture surface of sample OTS, **d** SEM of the crack growth of sample ITS, **e** EDS result of the position marked with the red cross in **d**

Fig. 9 Schematic diagram of high-temperature cracks generation of the FGM



in the matrix around Laves phase. As shown in Fig. 9, when the temperature was more than $0.65T_m$ (T_m = melting temperature), thermally activated deformation process for Laves phases would be promoted (Fig. 9a) [40], and thus facilitating the disintegrating of Laves phases during stretching process (Fig. 9b). Comparing with Figs. 4a and 8d, the morphology of Laves phases transformed from continuous stripes to dispersive granules after being stretched in 700°C . Ulteriorly during stretching process, the deformed small-sized Laves phase would be prone to induce stress concentration in the solid solution elements barren areas (Fig. 9c) [41]. Furthermore, due to low strength of the solid solution elements barren areas and the stress concentration, cracks would then occur around the Laves phases (Fig. 9d). Yet as for sample OTS, the graded region with high content of Laves has been eliminated by the optimized transition strategy, so the crack position of the FGM moved to the graded region with higher temperature tensile strength, contributing to the improvement of the high-temperature mechanical properties.

4 Conclusions

In this paper, optimized transition strategy was applied to improve the mechanical properties of Inconel625-HSLA steel functionally graded materials fabricated by WAAM. Microstructures, precipitation and mechanical properties in room temperature and 700°C were investigated. The conclusions are drawn in follows:

- (1) Inconel625-HSLA steel FGMs were fabricated in WAAM with iso-variable transition strategy and optimized transition strategy. The low-strength graded regions (70% HSLA steel-30% Inconel625 and 60% HSLA steel-40% Inconel625) and high Laves content graded regions (30% HSLA steel-70% Inconel625 and 40% HSLA steel-60% Inconel625) were eliminated by the optimized transition strategy.
- (2) In the FGM fabricated by optimized transition strategy, substantial MC-type Nb-rich carbides generated in the transition region between 50% HSLA steel-50% Inconel625 graded region and 80% HSLA steel-20% Inconel625 graded region, transferring the room-temperature crack position to graded region of 50% HSLA steel-50% Inconel625 and increasing the average room-temperature tensile strength from 449 to 509 MPa.
- (3) The solid solution elements barren areas and the stress concentration around which in the FGM fabricated by iso-variable transition strategy induced the cracks in high-temperature stretching.
- (4) Optimized transition strategy eliminated the high content Laves phases graded regions of the FGM, transferred the high-temperature crack position to graded region of 50% HSLA steel-50% Inconel625 and improved the average high-temperature tensile strength from 403 to 464 MPa.

Acknowledgements This work was supported by the National Natural Science Foundation of China (No. 52074191).

Conflict of interest On behalf all authors, the corresponding author states that there is no conflict of interest.

References

- G.P. Dinda, A.K. Dasgupta, J. Mazumder, *Mater. Sci. Eng. A* **509**, 98 (2009). <https://doi.org/10.1016/j.msea.2009.01.009>
- J. Nguejio, F. Szmytka, S. Hallais, A. Tanguy, S. Nardone, M. Godino Martinez, *Mater. Sci. Eng. A* **764**, 138214 (2019). <https://doi.org/10.1016/j.msea.2019.138214>
- A. Kreitchberg, V. Brailovski, S. Turenne, *Mater. Sci. Eng. A* **700**, 540 (2017). <https://doi.org/10.1016/j.msea.2017.06.045>
- R. Pamnani, T. Jayakumar, M. Vasudevan, T. Sakthivel, *J. Manuf. Process.* **21**, 75 (2016). <https://doi.org/10.1016/j.jmapro.2015.11.007>
- J. Tomkow, D. Fydrych, G. Rogalski, *Int. J. Adv. Manuf. Tech.* **109**, 717 (2020). <https://doi.org/10.1007/s00170-020-05617-y>
- R. Sridhar, K. Devendranath Ramkumar, N. Arivazhagan, *Acta Metall Sin. (Engl. Lett.)* **27**, 1018 (2014). <https://doi.org/10.1007/s40195-014-0116-5>
- H. Vemanaboina, G. Edison, S. Akella, *Mater. Res. Express.* **6**, 0965a9 (2019). <https://doi.org/10.1088/2053-1591/ab3298>
- N.K. Adomako, H.J. Park, S.C. Cha, M. Lee, J.H. Kim, *Mater. Sci. Eng. A* **799**, 140262 (2021). <https://doi.org/10.1016/j.msea.2020.140262>
- Y.L. Shi, S.K. Wu, H.B. Liao, X.Y. Wang, *J. Manuf. Process.* **54**, 318 (2020). <https://doi.org/10.1016/j.jmapro.2020.03.022>
- T. Ramkumar, M. Selvakumar, P. Narayanasamy, A. Ayisha Begam, P. Mathavan, A. Arun Raj, *J. Manuf. Process.* **30**, 290 (2017). <https://doi.org/10.1016/j.jmapro.2017.09.028>
- J. Zhang, X. Di, X. Jiang, C. Li, *Mater. Lett.* **316**, 132015 (2022). <https://doi.org/10.1016/j.matlet.2022.132015>
- M. Naebe, K. Shirvanimoghaddam, *Appl. Mater. Today.* **5**, 223 (2016). <https://doi.org/10.1016/j.apmt.2016.10.001>
- K. Swaminathan, D.M. Sangeetha, *Compos. Struct.* **160**, 43 (2017). <https://doi.org/10.1016/j.compstruct.2016.10.047>
- V. Chaudhary, M.S.K.K.Y. Nartu, S.A. Mantri, S. Dasari, A. Jagetia, R.V. Ramanujan, R. Banerjee, *J. Alloy. Compd.* **823**, 153817 (2020). <https://doi.org/10.1016/j.jallcom.2020.153817>
- C. Shen, Z. Pan, Y. Ma, D. Cuiuri, H. Li, *Add. Manuf.* **7**, 20 (2015). <https://doi.org/10.1016/j.addma.2015.06.001>
- T. Trosch, J. Ströbner, R. Völkl, U. Glatzel, *Mater Lett.* **164**, 428 (2016). <https://doi.org/10.1016/j.matlet.2015.10.136>
- T. Artaza, T. Bhujangrao, A. Suárez, F. Veiga, A. Lamikiz, *Metals* **10**, 771 (2020). <https://doi.org/10.3390/met10060771>
- T. Bhujangrao, F. Veiga, A. Suárez, E. Iriondo, F.G. Mata, *Crystals* **10**, 689 (2020). <https://doi.org/10.3390/cryst10080689>
- C.E. Seow, H.E. Coules, G. Wu, R.H.U. Khan, X. Xu, S. Williams, *Mater. Desgin* **183**, 108157 (2019). <https://doi.org/10.1016/j.matdes.2019.108157>
- J.F. Wang, Q.J. Sun, H. Wang, J.P. Liu, J.C. Feng, *Mater. Sci. Eng. A* **676**, 395 (2016). <https://doi.org/10.1016/j.msea.2016.09.015>
- Y. Li, Wu. Shaojie, H. Li, Y. Dong, F. Cheng, *Addit. Manuf.* **46**, 102124 (2021). <https://doi.org/10.1016/j.addma.2021.102124>
- W. Wu, J. Xue, Z. Zhang, P. Yao, *Mater. Manuf. Process.* **34**, 1502 (2019). <https://doi.org/10.1080/10426914.2019.1643473>
- L.D. Bobbio, B. Bocklund, R. Otis, J.P. Borgonia, R.P. Dillon, A.A. Shapiro, B. McEnerney, Z.K. Liu, A.M. Beese, *J. Mater. Res.* **33**, 1642 (2018). <https://doi.org/10.1557/jmr.2018.92>
- L.D. Bobbio, R. Otis, J.P. Borgonia, R.P. Dillon, A.A. Shapiro, Z.K. Liu, A.M. Beese, *Acta Mater.* **127**, 133 (2017). <https://doi.org/10.1016/j.actamat.2016.12.070>
- W. Meng, X. Yin, W. Zhang, J. Fang, L. Guo, Q. Ma, B. Cui, *J. Mater. Process. Tech.* **275**, 116368 (2020). <https://doi.org/10.1016/j.jmatprotec.2019.116368>
- C. Shen, X. Hua, M. Reid, K.-D. Liss, G. Mou, Z. Pan, Ye. Huang, H. Li, *J. Alloy. Compd.* **826**, 154097 (2020). <https://doi.org/10.1016/j.jallcom.2020.154097>
- S.R. Pulugurtha, Functionally graded Ti6Si4V and Inconel 625 by laser metal deposition, Ph.D. Thesis, Missouri University of Science and Technology (2014)
- F. Chen, M. Jia, Y. She, Wu. Yueqi, Q. Shen, L. Zhang, *J. Alloy. Compd.* **816**, 152512 (2020). <https://doi.org/10.1016/j.jallcom.2019.152512>
- Bo. Chen, Su. Yi, Z. Xie, C. Tan, J. Feng, *Opt. Laser Technol.* **123**, 105916 (2020). <https://doi.org/10.1016/j.optlastec.2019.105916>
- B.E. Carroll, R.A. Otis, J.P. Borgonia, J. Suh, R.P. Dillon, A.A. Shapiro, D.C. Hofmann, Z.K. Liu, A.M. Beese, *Acta Mater.* **108**, 46 (2016). <https://doi.org/10.1016/j.actamat.2016.02.019>
- J.R. Zhang, X.J. Di, C.N. Li, X.P. Zhao, L.Z. Ba, X. Jiang, *Metall. Res. Technol.* **118**, 502 (2021). <https://doi.org/10.1051/metal/2021063>
- A. Reichardt, R.P. Dillon, J.P. Borgonia, A.A. Shapiro, B.W. McEnerney, T. Momose, P. Hosemann, *Mater. Design* **104**, 404 (2016). <https://doi.org/10.1016/j.matdes.2016.05.016>
- Y. Wang, X. Chen, *Mater. Res. Express.* **6**, 106568 (2019). <https://doi.org/10.1088/2053-1591/ab39f6>
- A.N.M. Tanvir, M.R.U. Ahsan, Changwook Ji, W. Hawkins, B. Bates, D.B. Kim, *Int. J. Adv. Manuf. Tech.* **103**, 3785 (2019). <https://doi.org/10.1007/s00170-019-03828-6>
- T. Artaza, T. Bhujangrao, A. Suárez, F. Veiga, A. Lamikiz, *Metals* **10**, 771 (2020). <https://doi.org/10.3390/met10060771>
- F. Zhang, L.E. Levine, A.J. Allen, M.R. Stoudt, G. Lindwall, E.A. Lass, M.E. Williams, Y. Idell, C.E. Campbell, *Acta Mater.* **152**, 200 (2018). <https://doi.org/10.1016/j.actamat.2018.03.017>
- X.P. Zhao, X.J. Di, X. Zhang, C.N. Li, *Mater. Res. Express.* **8**, 066529 (2021). <https://doi.org/10.1088/2053-1591/ac0b0b>
- H. Nordberg, B. Aronsson, *J. Iron Steel Inst.* **12**, 1263 (1968)
- S. Matsuda, N. Okumura, *Trans. Iron Steel Inst. Jpn.* **18**, 198 (1978). <https://doi.org/10.2355/isijinternational1966.18.198>
- A. Von Keitz, G. Sauthoff, *Intermetallics* **10**, 497 (2002). [https://doi.org/10.1016/S0966-9795\(02\)00025-0](https://doi.org/10.1016/S0966-9795(02)00025-0)
- S. Sui, J. Chen, Z. Li, H.S. Li, X. Zhao, H. Tan, *Addit. Manuf.* **32**, 101055 (2020). <https://doi.org/10.1016/j.addma.2020.101055>

Publisher's Note Springer Nature remains neutral with regard to jurisdictional claims in published maps and institutional affiliations.